

Numerical modelling of reinforced concrete walls with minimum vertical reinforcement



Yiqiu Lu*, Richard S. Henry

Dept. of Civil and Environmental Engineering, University of Auckland, Auckland 1010, New Zealand

ARTICLE INFO

Article history:

Received 7 June 2016

Revised 14 February 2017

Accepted 15 February 2017

Keywords:

Reinforced concrete

Wall

Seismic design

Finite element model

Minimum vertical reinforcement

Strain hardening ratio

Drift capacity

Reinforcement buckling

Reinforcement fracture

ABSTRACT

Recent experimental results have shown that current minimum vertical reinforcement limits in many concrete design standards are insufficient to ensure that large ductility can be achieved during earthquakes. A detailed finite element model was developed in VecTor2 to provide a tool for further investigating the seismic behaviour of lightly reinforced concrete (RC) walls. The model was verified using experimental data from recent RC wall tests with minimum vertical reinforcement, and was shown to accurately capture both the overall response and local response parameters with good accuracy such as the cyclic hysteresis response, crack pattern, and vertical reinforcement strains. The model could also be used to estimate the drifts at which reinforcement buckling initiated and when reinforcement fractured occurred. The results from additional analyses showed that a potential size effect exists when considering the failure of lightly reinforced concrete walls. When keeping the reinforcement ratio and shear span ratio constant, the lateral drift capacity decreased significantly as the wall length increased. Using reinforcement with higher strength and lower ductility did not significantly impact the crack pattern, but did decrease the lateral drift capacity of the walls. Furthermore, reducing the strain hardening ratio of the reinforcement, or increasing the concrete strength, both resulted in a reduction in secondary cracking in the plastic hinge region and a reduced lateral drift capacity. It is recommended that wall length and average material properties should be accounted for when assessing the seismic behaviour of lightly reinforced concrete walls or when developing design standard requirements.

© 2017 Elsevier Ltd. All rights reserved.

1. Introduction

In regions of low or moderate seismicity, reinforced concrete (RC) walls with minimum vertical reinforcement are common when the dimensions of the wall are larger than that required for strength, or when axial loads provide sufficient flexural capacity. Recent research suggested that the minimum vertical reinforcement limits in the current version of the New Zealand Concrete Structures Standard, NZS 3101:2006 [1], may be insufficient to ensure that a large number of distributed cracks form in the plastic hinge region of RC walls [2]. A series of tests were recently conducted on six RC walls designed in accordance with the current minimum vertical reinforcement requirements in NZS 3101:2006 [3]. The test results confirmed that RC walls designed with minimum allowable distributed vertical reinforcement are unlikely to form a large number of secondary cracks in plastic hinge region, with the behaviour of the test walls controlled by 1–3 large primary flexural cracks at the wall base. The observed performance

of these six test walls was better than that observed in several lightly reinforced concrete walls that were damaged during the 2010/2011 Canterbury Earthquakes, where a single crack occurred at the wall base [4]. However, behaviour dominated by a limited number of wide flexural cracks can still lead to premature fracture of vertical reinforcement and low lateral drift capacities.

The tests conducted by Lu et al. [3] included six RC walls with identical dimensions that were approximately 40–50% of full-scale. Three parameters were varied during the tests, including shear span ratio, axial load, and anti-buckling ties. Other important variables such as wall dimension and scale, reinforcing steel properties, and concrete strength were not investigated during these tests. The effect of these parameters have been studied by numerous researcher for RC beams, however, there is limited existing research that highlights how these parameters influence the behaviour of RC walls with minimum vertical reinforcement. To investigate a wider range of parameters for lightly reinforced concrete walls, a numerical model capable of accurately capturing both the overall and local response was required. Despite extensive modelling techniques existing for RC walls, few numerical models have been developed or verified for flexure-dominant lightly

* Corresponding author.

E-mail address: ylu765@aucklanduni.ac.nz (Y. Lu).

reinforced concrete walls. Wibowo et al. [5] proposed a lumped plasticity model for lightly reinforced concrete walls for use as a simple design tool, but this technique does not model the local behaviour and so cannot accurately capture the crack distribution or lateral drift capacity when considering different failure modes.

The aim of this study was to develop a reliable model of lightly reinforced concrete walls that can accurately capture the overall lateral load response in addition to local response parameters such as crack pattern and reinforcement strains. A detailed finite element model was developed using plane stress membrane elements in VecTor2 and was verified against experimental results from recent tests on RC walls with minimum vertical reinforcement. Additional analyses were conducted using the developed model to investigate the effect of key parameters that were considered important for lightly reinforced concrete walls, but had not previously been investigated experimentally. Recommendations are provided regarding how these parameters should be accounted for when designing or assessing the seismic behaviour of lightly reinforced concrete walls.

2. Review of RC wall modelling

A large number of modelling approaches have been proposed for RC walls. These modelling approaches can generally be divided into four main categories: lumped plasticity models, macro models, distributed plasticity fibre element models, and continuum finite element models. Each modelling technique has advantages and disadvantages and may be suitable for different applications. To model the seismic behaviour and drift capacity of lightly reinforced concrete walls, it is important to capture both the overall lateral load response and local response parameters such as crack formation and reinforcement and concrete strains. Lumped plasticity models are simple and efficient but require extensive calibration with experimental data and can only predict the overall response rather than cracking and reinforcement strains at the wall base [5,6]. Distributed plasticity fibre based elements and macro models, such as truss models and multi-spring models, are shown to balance the efficiency of a simplified model and the refinements of a microscopic model. These models can accurately capture the lateral load response, energy dissipation, and stiffness degradation, and also local response parameters in ductile flexure dominant RC walls [7–10]. However, fibre element or macro models cannot accurately predict the behaviour of lightly reinforced concrete walls that exhibit limited flexural cracking and localisation of strains prior to and during failure. Continuum finite element models that use membrane, shell, or solid elements can provide the most detailed global and local response parameters in RC walls, but require increased computational effort and accurate multi-axial, nonlinear cyclic constitutive material models. When correctly implemented, finite element models can provide accurate estimation of RC crack development and local material strains [11–14].

VecTor2 [15] is a two-dimensional nonlinear finite element program specifically designed for modelling RC members. It implements both Modified Compression Field Theory [16] and the Disturbed Stress Field Model [17] to predict the response of elements subject to in-plane normal and shear stresses. Additionally, VecTor2 uses state-of-the-art material models that can account for compression softening, tension stiffening, tension softening, and tension splitting. In order to accurately capture both the overall response and local crack development, VecTor2 was selected for modelling lightly reinforced concrete walls.

VecTor2 has been used by numerous researchers to model the lateral load behaviour of RC walls. For example, Palermo and Vecchio [18] built VecTor2 models for both shear-dominant walls and

flexure-dominant walls. The comparison of modelling and test results showed that VecTor2 could capture overall response for both shear-dominant and flexure-dominant walls with reasonable accuracy. In addition, Model reports by Sritharan et al. [4] and Ghorbani-Renani et al. [12] showed that VecTor2 can accurately simulate the lateral-load response of flexure-dominant RC walls, including initial stiffness, shear deformations, energy dissipation, failure mechanisms, and cracking behaviour. Despite the suitability of VecTor2 for modelling lightly reinforced concrete walls, most previous studies have used it to model ductile RC walls with heavily reinforced end regions that generate well distributed secondary cracks. Luu et al. [13] used VecTor2 to model a slender 8-story lightly reinforced concrete wall with debonded reinforcement that was tested on a shake table and more recently Almeida et al. [19] built a VecTor2 model for a T-shaped lightly reinforced concrete wall with a total vertical reinforcement ratio of 0.51%. However, the walls considered by both of the studies were not representative of the lightly reinforced flexure-dominant concrete walls that exhibit discrete cracking behaviour. Validation of a numerical model capable of capturing the discrete flexural cracks and localisation of inelastic reinforcement strains was required to investigate a wider range of parameters for lightly reinforced concrete walls.

3. Finite element model

As discussed previously, VecTor2 [15] was selected for analysing lightly reinforced concrete walls that controlled by discrete cracking behaviour. Cracked concrete in VecTor2 is modelled as an orthotropic material using a smeared rotating crack approach where the cracks can re-orientate to align with the changing direction of the principal concrete compressive stress field [16]. The post-cracking rotation of the principal stress field is related to the post-cracking rotation of the principal strain field by a rotation lag [17]. Cracking strength is calculated depending on different stress states using Mohr-Coulomb Stress model [15]. In addition, crack shear-slip deformations are accounted for by relating shear slip along cracks to local shear stresses at cracks [20].

3.1. Model description

Diagrams of the lightly reinforced concrete walls tested by Lu et al. [3] and the corresponding models developed in VecTor2 are shown in Fig. 1. The test walls all had the same height, but were subjected to loading that represented three different shear span ratios equal to 2, 4 and 6. Test walls with a shear span ratio of 2 were subjected to horizontal force and axial load at the top of the wall, as shown in Fig. 1-a, while test walls with a shear span ratio of 4 or 6 were subjected a combination of horizontal force, axial load, and moment at the top of the wall, as shown in Fig. 1-c. The models were built for the test wall region with identical dimensions, material properties and vertical reinforcement details. For the walls with a shear span ratio of 2, a rigid beam element was used to model the steel loading beam and the loading height was the same as that of the test, as shown in Fig. 1-b. For the walls with shear span ratio larger than 2, a rigid region was also modelled to simulate the increased height of the prototype wall and to generate the same moment and shear actions at the top of the test wall, as shown in Fig. 1-d. For the model, the lateral displacement was applied on the top of the rigid region of the wall, but the lateral drift was monitored at the same height as the test walls to achieve a comparable lateral displacement loading protocol. For all the wall models, the axial load and lateral drift targets applied during the model analyses were identical to those applied to the test walls. Axial compression was applied at the top of the test wall region uniformly and held constant during the model analyses.

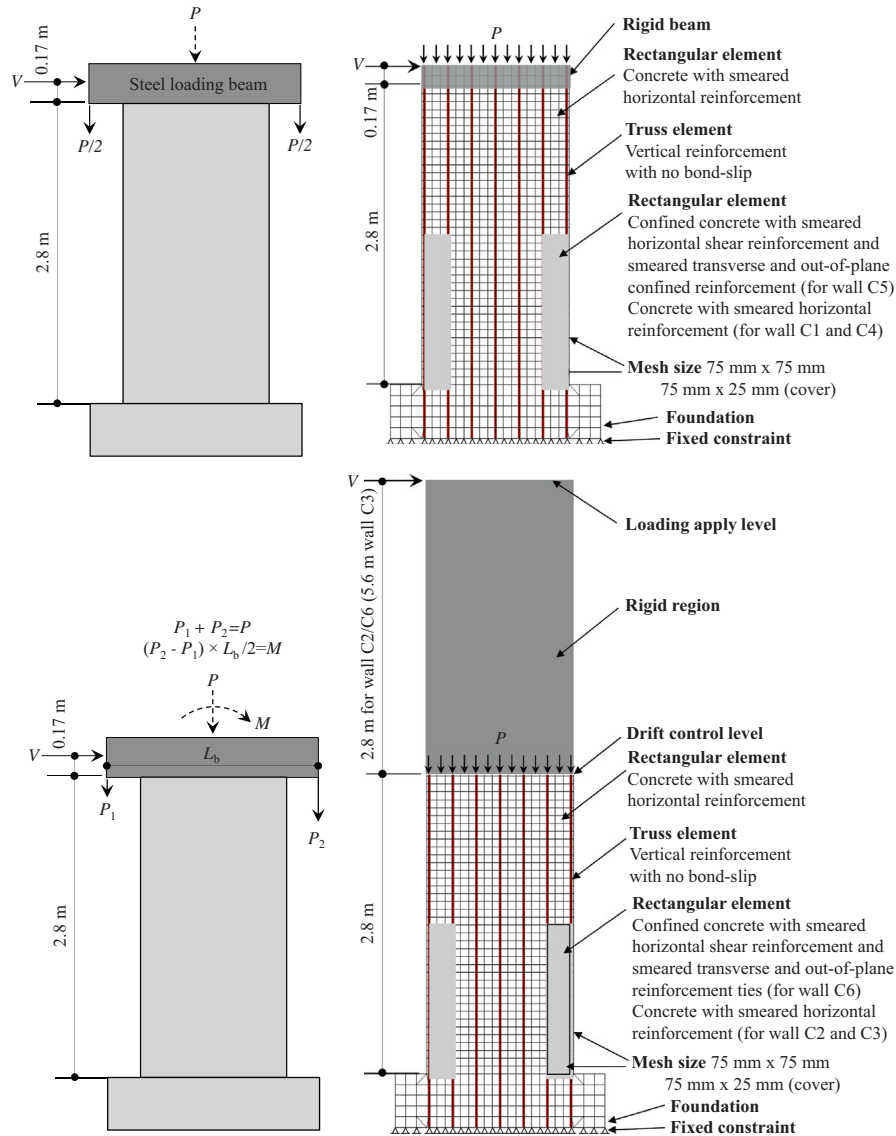


Fig. 1. Model illustration.

Four-node rectangular elements with a uniform thickness were used for the wall section. The horizontal shear reinforcement and additional transverse reinforcement ties were distributed uniformly over the wall height, and so were modelled as smeared reinforcement with an appropriate reinforcement ratio in either the transverse or/and out-of-plane directions. It should be noted that the legs of transverse reinforcement or anti-buckling ties were not accounted for in the model because of the 2D modelling technique adopted. The reinforcement ratio in the transverse or/and out-of-plane direction was calculated in accordance with the test specimens. For walls with transverse reinforcement ties in the ends of the wall, two different regions were modelled consisting of unconfined concrete with smeared horizontal shear reinforcement, and confined concrete with smeared horizontal shear reinforcement and smeared transverse and out-of-plane reinforcement ties, as shown in Fig. 1-b and d.

In order to discretely model the vertical reinforcement location and strains, two-node truss elements with uniform cross sectional area were used to represent each layer of vertical reinforcement. It was observed that the behaviour of all six test walls was controlled by 1–3 large flexural cracks at the wall base. The failure for all the

six test walls was controlled by vertical reinforcement buckling and subsequent reinforcement fracture, with no significant bond slip or longitudinal splitting observed during the test. Previous research has indicated that bond slip and yield penetration can be significant to the overall deformation of RC walls [21]. However, the model that did not include bond-slip was found to provide sufficient accuracy to capture the behaviour of the lightly reinforced test walls when using an appropriately refined mesh size. When concrete cracks, the reinforcement strain peaks at the location of the crack and the length of the yield penetration is typically estimated to be 3–5 times the reinforcement diameter on each side of the crack. Although perfect bond was assumed in the model, the stress and strains were averaged over the element length. The element size in the model was 75 mm which was equal to 7.5 times of the reinforcement diameter. By adjusting the mesh size the average strain was somewhat equivalent to the average strain in the test when considering the effects of reinforcement bond and yield penetration without having to include bond-slip elements.

The concrete foundation beam was also modelled at the base of the wall. The bottom edge of the foundation was fixed in the model

to represent the anchorage of the foundation to the laboratory strong floor. The vertical reinforcement in the wall extended continuously to the bottom of the foundation to simulate the anchorage of the reinforcement. The mesh size in the wall and foundation was chosen to be 75 mm × 75 mm as this size was found to best represent the wall behaviour after conducting a mesh sensitivity study. The mesh size used for the concrete cover was 25 mm × 75 mm as governed by the wall cover dimensions.

3.2. Steel constitutive model

The stress-strain response of the reinforcing steel implemented in the wall model used the nonlinear hysteric model proposed by Seckin [22], as shown in Fig. 2. The back-bone of the model included an initial linear-elastic response, a yield plateau, and a non-linear strain hardening phase until rupture (options HP4, P = 4 in VecTor2) [15]. The reinforcement used in the test walls was manufactured in coil form and so the yield plateau was lost when the reinforcement was straightened. Therefore, the strain hardening strain in the model was assumed to be equal to the yield strain to represent the lack of yield plateau. The reinforcement buckling model proposed by Dhakal and Maekawa [23] was implemented and the shear resistance due to dowel action was computed using Tassios Model [24]. Further details of the steel models that were used are available in the VecTor2 user manual [15].

Estimation of failure and ultimate drift capacity of structural members in finite element models often exhibits mesh sensitivity due to localisation of deformation at the controlling section. To accurately model the strength loss and drift capacity of lightly reinforced concrete walls where failure is typically controlled by reinforcement fracture, the model employed regularization of rein-

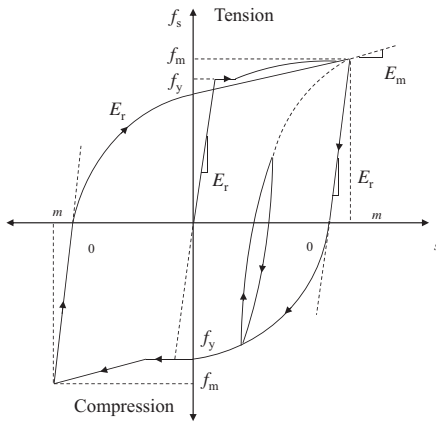


Fig. 2. Reinforcement constitutive model (after: Wong et al. [15]).

forcing steel material response using the steel yield energy and mesh-dependent lengths [25,26]. As shown in Fig. 3-a, the steel post-yield energy (G_{fs}) is defined as a function of material test data ($f_y, f_u, \epsilon_y, \epsilon_u$) and the gauge length used in material testing (l_{gauge}). As such, the regularized steel response model in which the regularized post-yield tangent stiffness ($b''E_s$) and regularized strain at ultimate strength (ϵ_u'') are functions of the steel post-yield energy (G_{fs}) that is determined from tensile tests and the integration (or mesh) length (l_{IP}), as shown in Fig. 3-b. The inputs for the reinforcing steel model in VecTor2 include yield strength (f_y), modulus of elasticity (E_s), ultimate strength (f_u), strain hardening strain (ϵ_{sh}) and ultimate strain (ϵ_u). The only parameter that altered during regularization was the ultimate strain, with the post-yield tangent stiffness adjusted by the program automatically.

3.3. Concrete constitutive model

The constitutive law for concrete in compression used the Hognestad parabola model for the ascending curve, with a Park-Kent [27] descending branch. The input peak concrete compressive strength for all the wall models in VecTor2 was based on the measured properties of the concrete as determined by compressive cylinder tests. The effect of confinement was considered by using a strength enhancement factor, β_1 , which is calculated by the Kupfer/Richard confinement strength model [28,29] using the input transverse and out-of-plane reinforcement ratio. The value of β_1 served to modify the concrete compression response curves by increasing both the uniaxial compressive strength, f'_c , and corresponding strain, ϵ_0 , to determine the peak compressive strength, f_p , and corresponding strain, ϵ_p . The model proposed by Lee et al. [30] was chosen to represent the concrete tension stiffening, with the peak concrete tensile strength for all the test wall models determined from split cylinder tests. The method of using split tensile strength to be concrete tensile strength is in accordance with the *fib* model code recommendation [31], in which the conversion factor from the mean axial tensile strength to the mean splitting tensile strength is assumed to be 1.0. The cyclic parameters in the concrete stress-strain model were based on that proposed by Palermo and Vecchio [18] and crack slip was taken into account according to the Vecchio-Lai model [20]. The cyclic hysteric response for the concrete model in compression is shown in Fig. 4. VecTor2 does not currently incorporate a crack-closure model so it was not able to be included in the proposed model.

4. Model calibration and verification

To examine the suitability of the VecTor2 model for lightly reinforced concrete walls, the model was verified against available

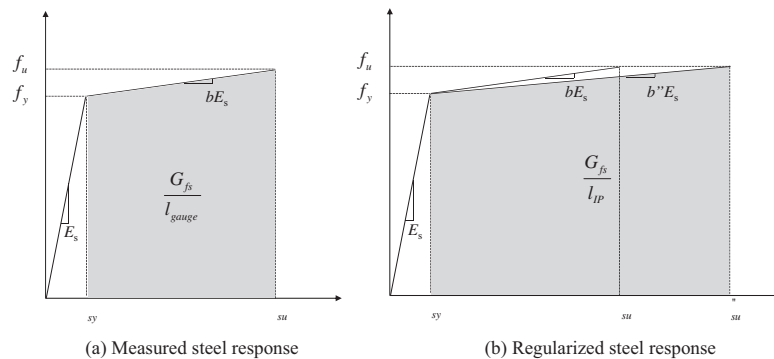


Fig. 3. Measured and regularized stress-strain response of reinforcement (after: Pugh et al. [26]).

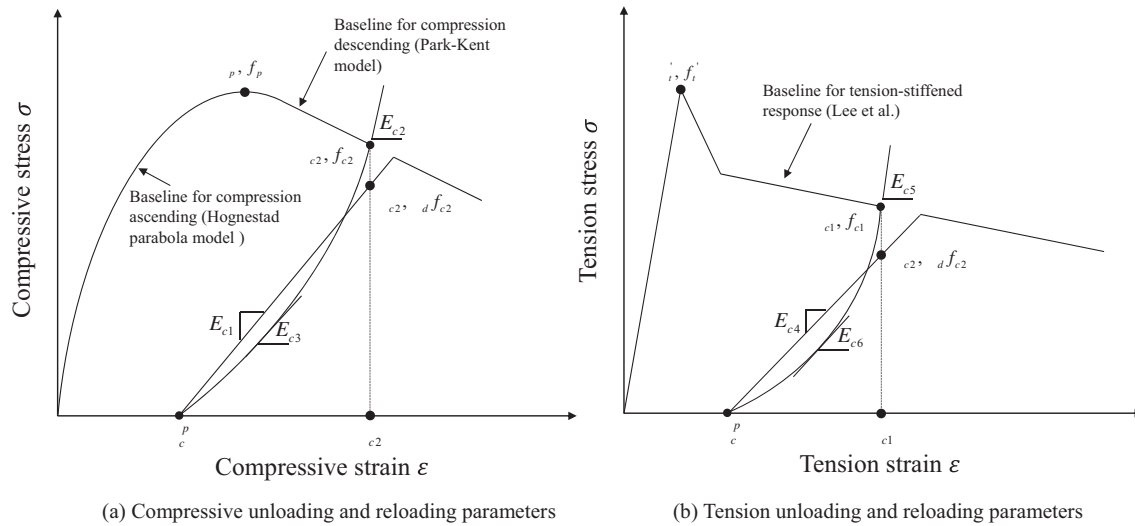


Fig. 4. Hysteretic response of concrete models (after: Wong et al. [15])

Table 1
Details of all six test walls.

Wall	Shear span ratio (M/Vl_w)	Axial load ratio	Concrete compressive strength f'_c (MPa)	Concrete tensile strength f'_t (MPa)	Vertical reinforcement ratio (%)	Horizontal reinforcement ratio (%)	End ties (mm)
C1	2	3.5%	38.5	2.88	0.53	0.25	None
C2	4	3.5%	34.5	2.53	0.53	0.25	None
C3	6	3.5%	36.2	3.05	0.53	0.25	None
C4	2	0	34.7	2.65	0.53	0.25	None
C5	2	6.6%	35.4	2.81	0.53	0.25	R6@90
C6	4	3.5%	37.3	2.81	0.53	0.25	R6@60

experimental results. The six RC walls tested by Lu et al. [3] were chosen to verify the model as they represented typical lightly reinforced concrete walls and had extensive data of the measured wall response. An overview of the test wall details that was required to build the model and the subsequent calibration and verification are presented below.

4.1. Test wall description

A summary of the main parameters for the six test walls is shown in Table 1, and drawings of the wall specimens are shown in Fig. 5. The test walls had a length of 1.4 m, height of 2.8 m and a thickness of 150 mm. The total vertical reinforcement ratio was 0.53%, resulting in $14 \times D10$ (deformed G300E, diameter = 10 mm) bars placed in two layers at 225 mm centers over the wall length. R6 (plain G300E, diameter = 6 mm) stirrups were used for horizontal reinforcement distributed evenly at 150 mm centers over the wall height. Most of the test walls did not have transverse stirrups or ties at ends of the wall, except for walls C6 and C5 that had R6 stirrups placed at 60 mm and 90 mm centers, respectively, over the lower 1.4 m of the wall height. Grade 300E New Zealand reinforcing steel was used in the test walls. The D10 reinforcement had a measured yield strength of 300 MPa, an ultimate strength of 409 MPa, and an ultimate strain at fracture of 18.1%. The R6 reinforcement had a measured yield strength of 300.6 MPa, an ultimate strength of 461.8 MPa, and an ultimate strain at fracture of 12.6%. The specified concrete (f'_c) was 40 MPa and the measured concrete mechanical properties at the time of testing of all six walls at the time of each test are listed in Table 1. Further details including foundation design, test setup used to achieve a varied shear span ratio, and instrumentations for measuring top lateral displacement,

axial strains, panel deformation components, and reinforcement strain are published separately [3].

4.2. Model development

The sensitivity of the mesh size was considered to be critical to the accuracy and interpretation of the wall model, and was investigated in detail during the model development. The mesh size greatly influences the resolution of the local strains and can affect the calculation of failure due to localisation if the material models are not regularised correctly. Trial models were run to investigate the sensitivity of the mesh size to the analysis results. To illustrate the conclusions from this sensitivity study, the results of two different mesh sizes, 150×150 mm and 75×75 mm, are compared. In all cases, the mesh size was chosen to allow for direct comparison of the model to the vertical reinforcement strains that were measured over a gauge length of 150 mm during the tests.

A comparison of model results for test wall C1 using mesh sizes of 150×150 mm and 75×75 mm are shown in Fig. 6. The global base moment-displacement response for the models with both mesh sizes correlated well with the test response up until a lateral drift of 1.5%. The model with mesh size of 75 mm was able to capture the energy dissipation and strength loss during lateral drift cycles to 2.0% and 2.5% with improved accuracy. However, it should be noted that both models could not accurately capture the strength degradation during cycles to 2.0% and 2.5% lateral drift and the pinching behaviour of the test walls. These discrepancies were attributed to the limitation of the material models used in VecTor2 as discussed below in more detail and were not affected by the mesh size. The global responses of both models were similar and the mesh size of 150×150 mm was sufficient to simulate the

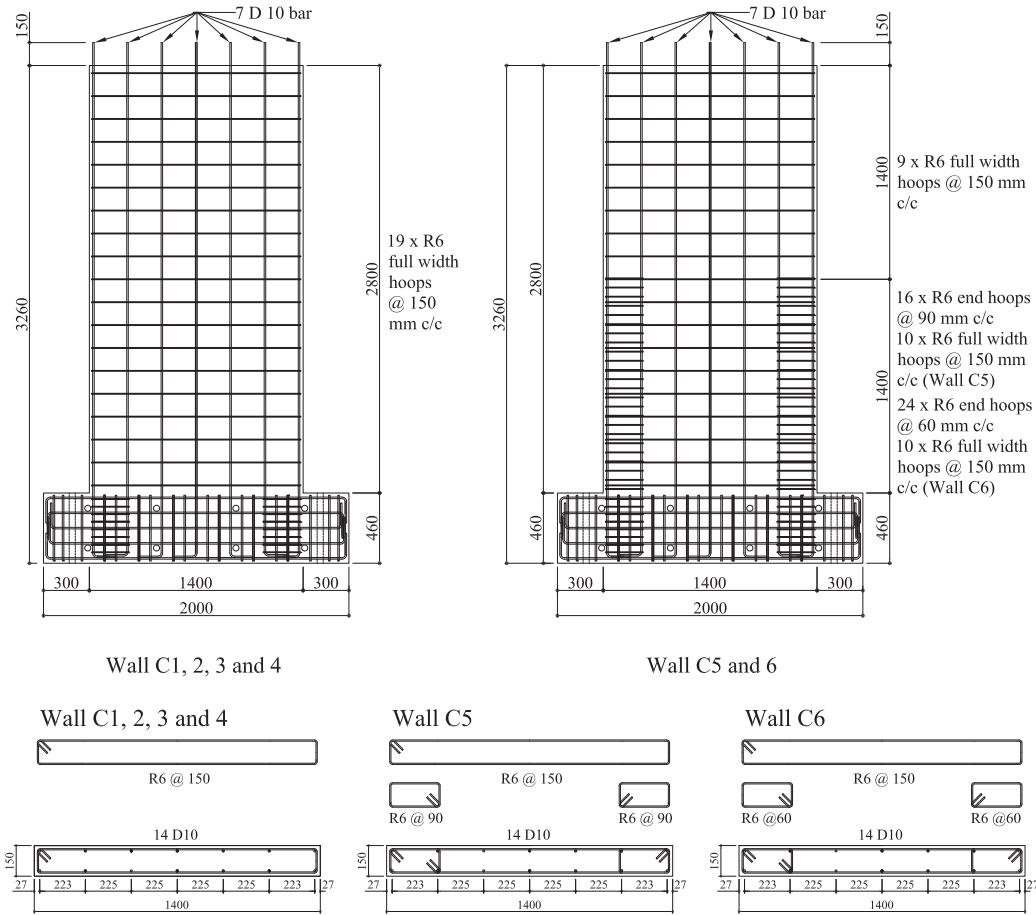


Fig. 5. Details of test wall specimens.

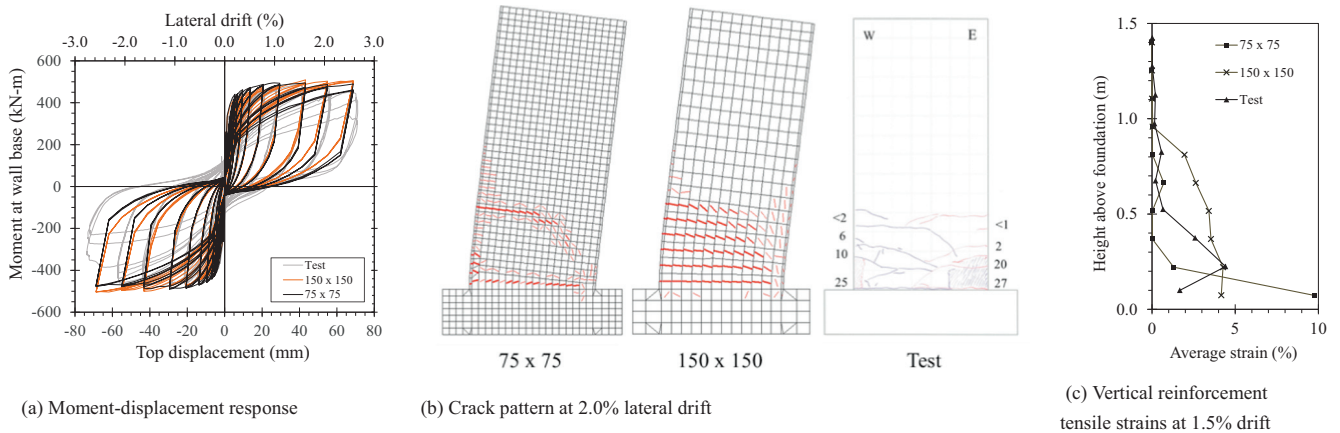


Fig. 6. Comparison of models of wall C1 with mesh sizes of 150 mm and 75 mm.

global wall response. Despite a similar global response, the predicted crack patterns and vertical reinforcement strains varied substantially between the models with different mesh sizes, as shown in Fig. 6-b and c. The model with mesh size of 75 mm was able to capture the dominant discrete cracking that was observed during the test, with two large primary flexural cracks predicted at the base of the wall. In contrast, the 150 mm mesh size was too coarse to capture the formation of discrete primary flexural cracks, an instead a large number of cracks at all mesh layers formed in the lower portion of the wall. As a result of these different crack patterns the reinforcement strains in the model with a

150 mm mesh were more evenly distributed over the plastic hinge length, whereas the refined 75 mm mesh captured the concentration of inelastic strains that occurred at the wide discrete cracks in the wall. Consequently, the model mesh size of 75 mm provided a better estimation of the test wall behaviour and was considered refined enough to capture the local response. Furthermore, after the mesh size was refined to capture both the global and local wall response, regularization of reinforcing steel model inputs was employed to achieve accurate mesh-objective simulation of drift capacity, as described earlier in the model description [25]. Based on the results of the mesh sensitivity study, a mesh size of

75 × 75 mm was chosen for the proposed model of lightly reinforced concrete walls. The average ultimate strain measured from tensile test samples was 18.1% using a gauge length of 100 mm. Therefore, the regularized ultimate strain at fracture (the input of ultimate strain in VecTor2) was 24.2% based on a mesh size of 75 mm using the regularization technique described earlier. For the regions of confined concrete, the mesh size did not influence the overall and local behaviour significantly as lightly reinforced concrete walls studied herein were controlled by vertical reinforcement fracture and significant concrete crushing did not occur. Therefore, a mesh size of 75 × 75 mm was also used in the confined concrete regions for consistency with other regions of the wall.

4.3. Experimental Validation

The VecTor2 model was run for all six walls tested by Lu et al. [3]. The calculated model results were compared with the test results in terms of overall moment-displacement response, crack pattern, and reinforcement strains to establish the accuracy and limitations of the model.

4.3.1. Moment-displacement response

A comparison of the measured and calculated base moment-displacement responses for all six test walls is shown in Fig. 7. Overall, the model captured the measured response of the test walls reasonably well. The strength and stiffness of the walls were accurately calculated for most lateral drift cycles and the cyclic hysteresis response was also closely matched for most walls. In particular, the model accurately captured the strength and stiffness degradation on subsequent cycles. Non-linear shear deformations were observed during the test and the model was able to predict these shear deformations with good accuracy. However, the shear

deformations in all the six test walls were extremely small when compared to the flexure deformation (typical less than 5%) [3], and so the shear deformations were not considered significant to the model verification. The inaccuracy of the model with regards to strength degradation beyond 1.5% lateral drift and the pinching in the hysteretic response are discussed below in more detail.

4.3.2. Crack patterns

The crack patterns documented during the six wall tests are compared against the calculated crack patterns from the model at 1.5% lateral drift in Fig. 8

Fig. 8, the drift level of 1.5% was close to the point at which the peak lateral strength was reached prior to degradation caused by reinforcement buckling and fracture. Considering that the observed crack patterns were often affected by various experimental and specimen uncertainties, the model crack patterns were considered to provide a reasonable representation of the observed wall behaviour. For example, the behaviour of the test walls was controlled by 3–4 main primary cracks with the bottom crack opening the widest and dominating the response. In the model, the crack pattern was also controlled by a small number of primary cracks, with the bottom primary crack opening significantly wider than the second primary crack. Both in the test and the model, the top lateral deformation was mostly attributed to the widest crack at the wall base. Moreover, the height over which the cracks extended up the wall in the test was also well captured by the model. During the test, it was observed the cracks extended higher up the height of the wall as a result of the higher shear span ratio. Similar behaviour can also be found in the model, as shown in Fig. 8. These results indicated that the model can sufficiently predict the crack pattern of lightly reinforced concrete walls with discrete flexural cracks.

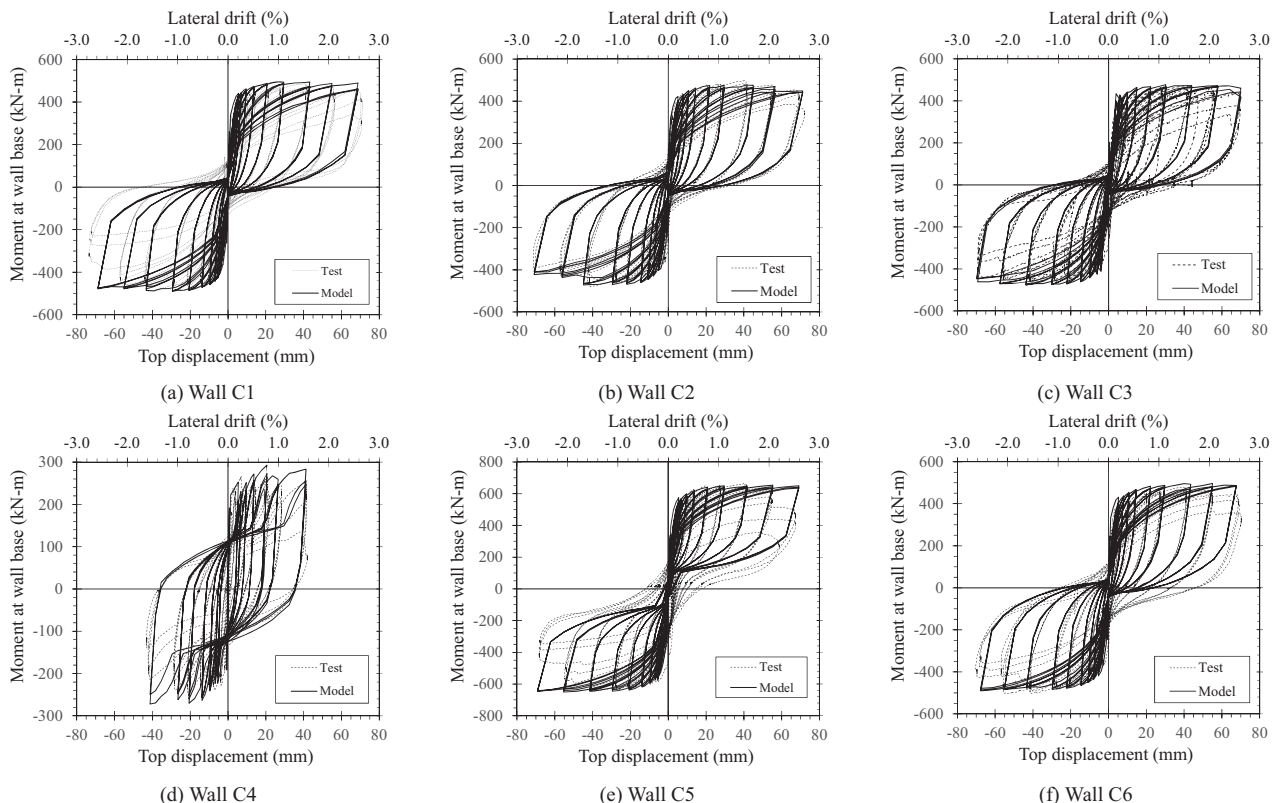


Fig. 7. Comparison of moment-displacement response for all six test walls.

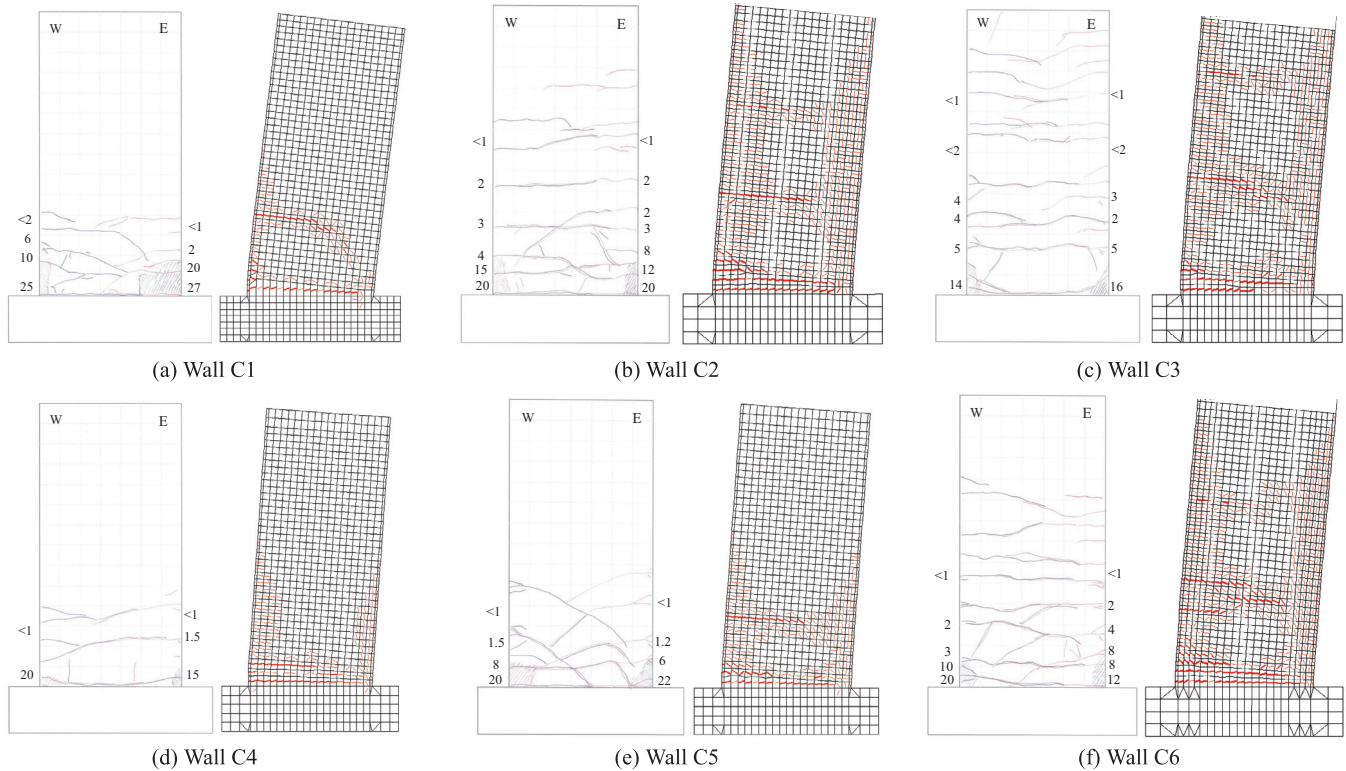


Fig. 8. Comparison of crack patterns for all six test walls.

4.3.3. Reinforcement and concrete strains

Comparisons between the measured and modelled reinforcement strains in the extreme tension reinforcement over the wall height at 1.5% lateral drift are shown in Fig. 9 for all six walls. The drift of 1.5% was chosen for the comparison as the displacement gauges that were used to measure reinforcement strains were compromised after 1.5% lateral drift when reinforcement buckling occurred. The strains measured during the test were based on the gauge length of 150 mm. Therefore, the strains extracted from the model were also the average strains over a 150 mm mesh length (two 75 mm elements). When considering that the experimental results were often affected by various experimental and specimen uncertainties, such as the crack distribution, the model results are considered to be in reasonable agreement with the measured strains. The test result showed that instead of the reinforcement tensile strains yielding consistently over the entire plastic hinge region, large concentrations in reinforcement strains were observed at location of wide flexural cracks. As shown in Fig. 9, the model was also able to capture this irregular strain profile. The peak reinforcement strains were slightly overestimated by the model, but these differences were considered acceptable knowing that a small difference in stress produces a large variation in strain in the post-yield region.

An example comparison between the measured and modelled concrete compressive strains at the wall edge during cycles to 1.0% lateral drift (before concrete spalling or reinforcement buckling) are shown in Fig. 10 for wall C1. The strains measured during the test were based on externally mounted displacement sensors with a gauge length of 150 mm. Therefore, the strains extracted from the model were also the average strains over a 150 mm mesh length (two 75 mm elements). The measured compressive strains showed a more consistent trend up the wall height when compared to the reinforcement tensile strains, with a peak strain at wall base of approximately 0.005 at 1% lateral drift. The model

was able to capture the concrete compression strains with good accuracy, closely matching both the peak strains at the wall base and the trend up the wall height.

4.3.4. Reinforcement buckling

Despite reasonable accuracy overall, the model could not accurately capture reinforcement buckling. Strength and stiffness degradation in the measured response of the test walls occurred during cycles to 2.0% and 2.5% lateral drift due to buckling of the vertical reinforcement. The VecTor2 model did consider reinforcement buckling using a model based on compression stress in the reinforcement and the ratio of the unsupported length to bar diameter L/D [15], but this model was insufficient to capture the buckling observed during the test. The test results highlighted that the vertical reinforcement in the test walls was particularly vulnerable to buckling because of the wide flexural cracks that dominated the behaviour of these lightly reinforced concrete walls, resulting in concentrations of tensile strain in the vertical reinforcement. This behaviour was also highlighted by Moyer and Kowalsky [32] and Restrepo-Posada [33] who suggested that the strain limit for initiation of reinforcement buckling should also be related to the tension strain on the previous load cycle. For example, in wall C4 the compressive strain of vertical reinforcement was small but the tensile strain was large due to the lack of axial load and light vertical reinforcement content. During the test of wall C4, the vertical reinforcement started to buckle during the first cycle to a lateral drift of 0.75%, but the model did not predict buckling of vertical reinforcement because the compressive yield strain of the reinforcement was not reached. Fig. 11-a shows the calculated stress-strain response of the outmost vertical reinforcement in the model of wall C4 during cycles to 1.5% lateral drift. The stress of vertical reinforcement did not drop when the reinforcement was subjected to compression, implying that no buckling had occurred despite tensile strains in excess of 5%. In the model of wall C2, rein-

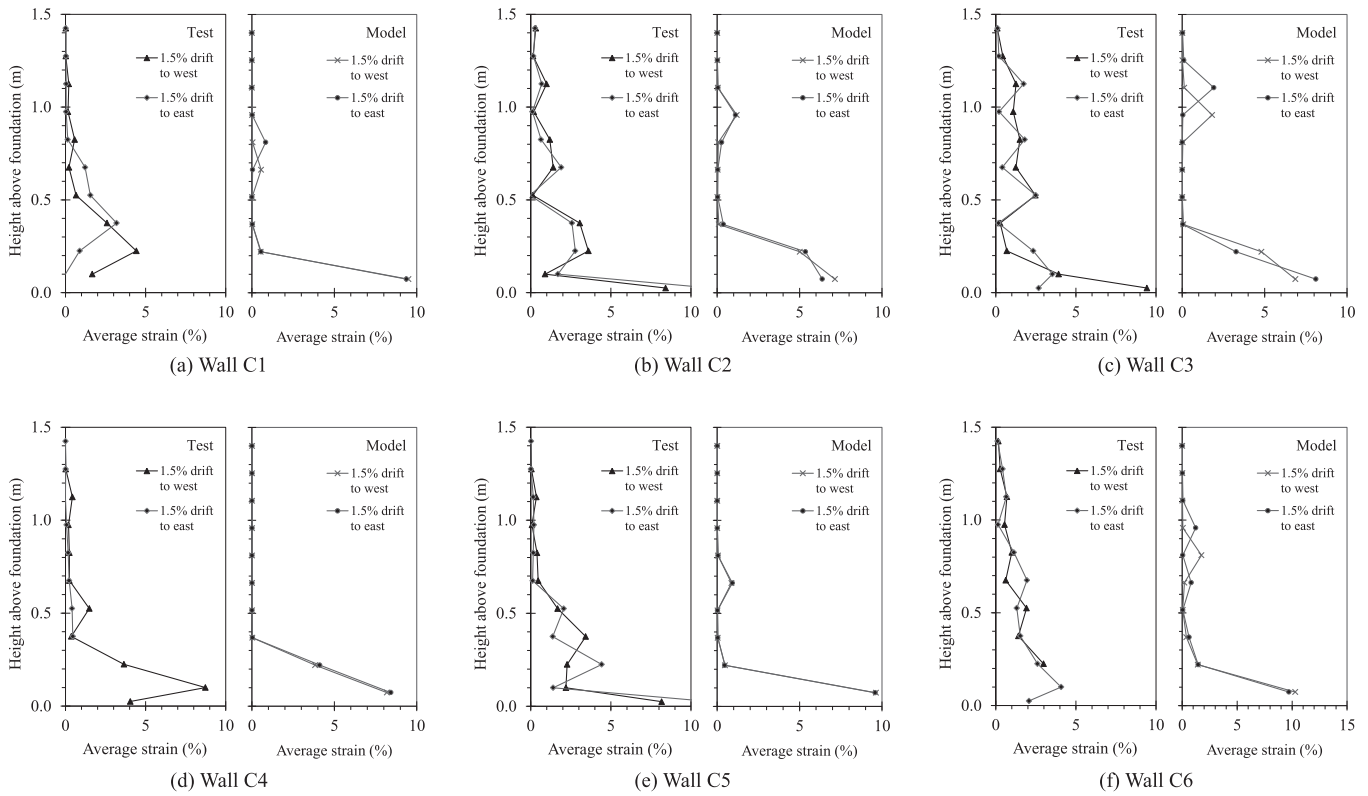


Fig. 9. Comparison of vertical reinforcement strains for all six test walls.

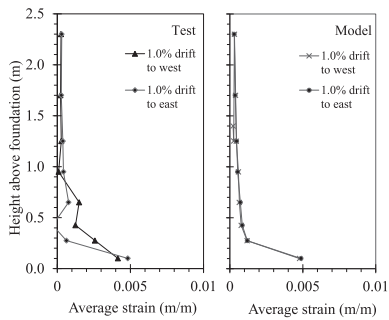


Fig. 10. Comparison of vertical concrete compressive strains for wall C1.

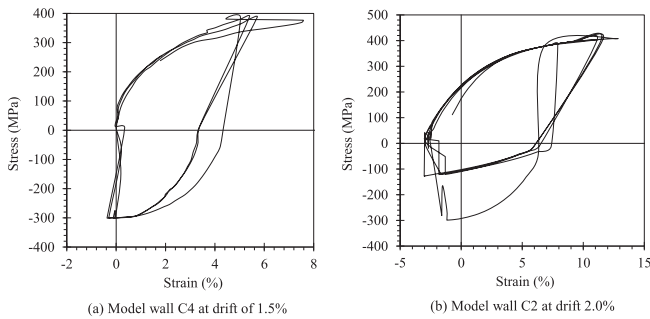


Fig. 11. Stress-strain relationship of outmost vertical reinforcement in model wall C4 and C2.

forcement buckling occurred during cycles to 2.0% lateral drift, as shown by the calculated stress-strain response in Fig. 11-b. However, the vertical reinforcement buckling occurred earlier at a lateral drift of 1.5% during the test, confirming that the model could not accurately represent the reinforcement buckling in these walls.

4.3.5. Residual drift

For most walls the cyclic response was captured with reasonable accuracy. However, for some walls the residual drift and reloading stiffness were not well captured. For example, the calculated moment-displacement response for the model of wall C5 followed a flag shape, with significantly less hysteretic energy dissipation and residual drift than the test wall response, as shown in Fig. 7-e. This discrepancy in the model was due to the cyclic concrete material model in VecTor2 not accounting for the crack closure behaviour, with the compressive stresses not developing until the tension strain has unloaded to zero. Fig. 12 shows the calculated stress-strain response of a concrete element in the corner of the wall C5. The unloading and reloading branches passed through the origin, indicating no compression stress developed until the crack was fully closed (zero strain). This is unrealistic due to the presence of crushed concrete in open cracks, leading

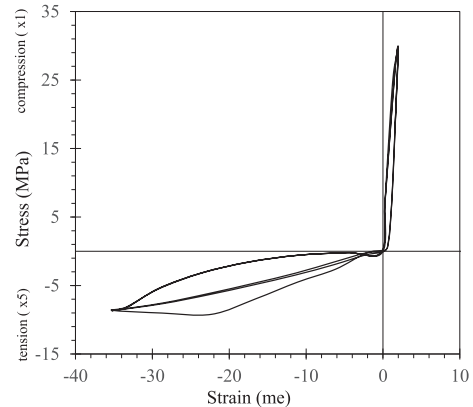


Fig. 12. Stress-strain curve of the concrete element at bottom horizontal row and second vertical row in wall C5 during the drift of 0.35%.

to underestimation of energy dissipation and residual displacement at zero load. It should be noted that the calculated residual displacement and energy dissipation of wall C4 which had zero additional axial load applied agreed well with the test results. The effect of the crack closure model was less profound for walls with lower axial load which were insufficient to close the open cracks at zero lateral load even though the concrete closure model was not considered. The mismatching caused by concrete crack closure model has been observed in other RC wall models and was examined in detail by Waugh et al. [34]. Improved model results can be achieved using a concrete model that account for the transition between crack opening and closure, such as the Chang and Mander's model [34,35]. However, VecTor2 does not currently implement such a model and so this behaviour was not represented by the analytical model.

Inaccuracies in capturing the peak reinforcement strains at cracks may have also contributed to the discrepancy in calculated and measured residual drifts. As discussed previously, the model can reasonably predict the reinforcement strain profile. However, there were still some spikes that were not well captured by the model which would add to ratcheting of reinforcement and an accumulated residual displacement. Overall, the calculation of residual drift was not considered essential to achieve the objective of the model and the cyclic hysteresis response was not relied on during the additional analyses reported below.

4.3.6. Estimation of drift capacity

Buckling and subsequent fracture of the vertical reinforcement controlled the failure of all six test walls. As described previously, the reinforcement buckling model did not accurately predict the initiation of vertical reinforcement buckling due to the reliance of the model on compressive strains, whereas the reinforcement buckling in the tests was attributed to large tensile strains at cracks. The tensile strain at the buckling location measured during the tests in the drift cycle prior to reinforcement buckling and the corresponding peak strains calculated from the model during the same drift cycle are shown in Table 2. The gauge length for measuring reinforcement strains during the test was 150 mm except that the lowest two gauges had a length of 100 mm and 50 mm respectively. If the reinforcement buckling occurred at the location of the lowest two gauges, the measured tensile strain was calculated as the average of the lowest two gauges with a gauge length of 150 mm to be consistent with other gauges. The calculated reinforcement strains were also based on a gauge length of 150 mm (two 75 mm elements). It should be noted that the model itself was calculated based on a mesh size of 75 mm which predicts better strain localization behaviour. The gauge length of 150 mm was only used when extracting the reinforcement strain results for comparison with test results. As shown by the results in Table 2 the reinforcement tensile strains prior to reinforcement buckling were consistent for both the test and

model. For the test wall, the peak reinforcement tensile strains in the cycle prior to buckling ranged from 2.2% to 4.4% with an average of 3.93 and 3.5 and coefficient of variation of 0.07 and 0.22 for east and west ends, respectively. The corresponding calculated reinforcement strains ranged from 6.4% to 10.2% with a coefficient of variation of 0.16 at both the east and west ends. Furthermore, the ratio between the calculated tensile strain and the measured tensile strain was also consistent, with an average of 2.04 and 2.34 and a coefficient of variation of 0.10 and 0.21 for east and west ends, respectively. Although the reinforcement tensile strain prior to buckling was overestimated by the model due to the exact crack pattern and location of reinforcement buckling, the onset of reinforcement buckling could still be estimated with reasonable accuracy when the calculated reinforcement tensile strain at wall base exceeded 8% based on a gauge length of 150 mm.

Although the model could capture the discrete cracking behaviour and strain localization with reasonable accuracy when using a 75 mm element size, the peak reinforcement strains were not accurately predicted. In addition, it was found that reinforcement buckling was critical to the initiation of fracture during test, which could not be captured in VecTor2. For these reasons, reinforcement fracture could not be predicted directly by the model. However, a method to estimate drift capacity when reinforcement fractured was developed based on the ultimate strain estimated from direct tension test of reinforcement samples. For consistency with the gauge length used to estimate the drift at which reinforcement buckling initiated, the reinforcement strain used to estimate the drift capacity at which reinforcement fractured was also based on a 150 mm length (two element size). The average ultimate strain measured from tensile test samples was 18.1% using a gauge length of 100 mm. If the effects of low-cyclic fatigue and reinforcement buckling are ignored, the ultimate strain indicating reinforcement fracture in the model can be estimated as 12.1% (ϵ_{reg}) based on a gauge length of 150 mm using the regularization technique described earlier. The calculated tensile strain from the model at the drift that reinforcement fractured in the test is compared against the regularised ultimate strain capacity in Table 3 for each wall. The calculated reinforcement strain when the reinforcement fractured correlated well with the 12.1% strain capacity. The ratio between the calculated tensile strain at the drift that reinforcement fractured and the regularised tensile strain capacity ranged from 0.68 to 1.28 with an average of 0.98 and 0.94 for east and west ends, respectively. Therefore, the ultimate drift capacity can be reasonably estimated based on the calculated tensile strains at wall base reaching the regularised strain limit of 12.1% for a 150 mm gauge length.

In summary, the drift capacity at which reinforcement buckling and fracture occurred could both be reasonably estimated when the calculated tensile strain at the wall base exceeding 8.0% and 12.1%, respectively, based on a gauge length of 150 mm.

Table 2
Comparison of vertical reinforcement tensile strain prior to reinforcement buckling.

Wall	Drift at buckling (%)		Test tensile strain prior to buckling (%)		Model tensile strain (%)		Comparison	
	Drift to east	Drift to west	Drift to east	Drift to west	Drift to east	Drift to west	Drift to east $\epsilon_{model}/\epsilon_{test}$	Drift to west $\epsilon_{model}/\epsilon_{test}$
C1	1.5	1.5	4.4	2.2	9.3	7.0	2.11	3.18
C2	1.5	1.5	3.6	2.8	6.4	7.1	1.78	2.54
C3	1.5	1.5	3.6	3.5	6.8	6.7	1.89	1.91
C4	0.75	1.0	3.9	4.2	7.5	7.5	1.92	1.79
C5	1.5	1.5	4.0	4.4	9.1	9.1	2.30	2.07
C6	2.0	1.5	4.1	3.9	9.7	10.2	2.37	2.62
Average			3.93	3.50	8.08	7.90	2.06	2.35
COV			0.07	0.22	0.16	0.16	0.10	0.21

5. Effect of key parameters

Section dimensions and material properties were regarded as key parameters when developing the minimum longitudinal reinforcement requirement for RC beams and plates [36,37]. In addition, the observation of lightly reinforced concrete walls from recent tests [3] and during the 2010/2011 Canterbury Earthquakes in New Zealand [38] indicated that both wall length and material properties may significantly influence wall cracking behaviour and drift capacity. To further study the effect of these parameters to the behaviour of lightly reinforced concrete wall, the developed VecTor2 model was used to investigate the lateral load response of walls with different dimensions and material properties to that of the six test walls. A total of eleven additional walls were modelled to investigate the effect of wall dimension, reinforcement type, and concrete strength. Details of the additional walls modelled are summarised in Table 4. The selected baseline wall for comparison was test wall C1 with a shear span ratio of 2 and an axial load ratio of 3.5%. All the walls modelled used the same loading and lateral drift protocol as that of test wall C1. The drift capacity was compared for each model assuming that reinforcement fracture controlled the failure irrespective of whether reinforcement buckling was expected to occur. As discussed previously, the onset of reinforcement fracture was defined as vertical reinforcement tensile strain exceeding 12.1%.

5.1. Size effect

When the wall behaviour is dominated by a discrete number of wide flexural cracks, the plastic hinge rotation at which certain crack widths occur will be a function of the wall length, as illustrated by the example in Fig. 13. The wall test results suggested that the crack widths were consistently about 20 mm when the reinforcement fractured [3]. The length of the test walls was only 1.4 m due to the 40–50% scale of the specimen. If the wall was full scale, the wall base rotation and the drift capacity at which a

20 mm crack formed, and reinforcement fracture occurred, would be expected to be approximately half that of the scaled test wall. However, this hypothesis proposed by Lu et al. [3] was based on the observation from six lightly reinforced concrete wall tests and was not previously verified by any test or modelling results. In this study, the model was calibrated to predict the moment-displacement response, cracking behaviour and localisation of reinforcement strains by using an appropriately refined mesh size and to provide mesh objective estimates of drift capacity by employing regularization of the reinforcing steel model. Therefore, the model was considered suitable for capturing any potential size effect that may occur for lightly reinforced concrete walls.

The dimensions of the two larger walls C1-1 and C1-2 were $225 \times 2100 \times 4200$ mm (1.5 times of C1) and $300 \times 2800 \times 5600$ mm (2 times of C1), respectively. When the walls had larger dimensions, either reinforcement spacing or the number of reinforcing bars could be adjusted to keep the reinforcement ratio consistent with the baseline wall C1, resulting in two alternative reinforcement layouts for each modelled wall. Wall C1-1a used two layers of D15 reinforcement at 338 mm centers and wall C1-1b used two layers of D11.1 reinforcement at 225 mm centers. Wall C1-2a used two layers of D20 bars at 450 mm centers and wall C1-2b used two layers of D14.7 bars at 225 mm centers. All other parameters including shear span ratio, axial load and material properties for walls C1-1a, C1-1b, C1-2a and C1-2b were consistent with that of wall C1.

The reinforcement strains in the extreme vertical tension reinforcement and the envelope of the cyclic moment-displacement response of the five walls are compared in Figs. 14 and 15, respectively. As shown in Fig. 14, the reinforcement strain distributions were similar for all walls, indicating wall dimension did not change the crack pattern significantly. However, the peak reinforcement strains at the wall base increased as the wall size increased. For example, at a lateral drift of 0.5%, the maximum reinforcement strains for walls C1, C1-1a and C1-2a were 3%, 4.6% and 5.4%, respectively. Therefore, the larger walls experienced reinforcement

Table 3
Comparison of vertical reinforcement strain at reinforcement fracture.

Wall	Drift when fracture occurred during test (%)		Model peak tensile strain at drift when fracture occurred, ϵ_{model} (%)		Comparison	
	Drift to east	Drift to west	Drift to east	Drift to west	Drift to east $\epsilon_{model}/\epsilon_{reg}$	Drift to west $\epsilon_{model}/\epsilon_{reg}$
C1	2.5	N/A	15.5	N/A	1.28	N/A
C2	2.5	2.5	8.5	8.9	0.70	0.74
C3	2.5	2.5	13.4	14.5	1.11	1.20
C4	1.5	1.5	8.4	8.2	0.70	0.68
C5	2.0	2.0	12.7	12.8	1.05	1.06
C6	2.5	2.0	12.6	12.4	1.04	1.02
Average			11.7	11.3	0.98	0.94
COV			0.22	0.21	0.22	0.21

Table 4
Details of modelled walls.

Wall No.	Main parameter	Dimensions (mm)	Reinforcement properties					Concrete properties	
			Type	f_y (MPa)	f_u (MPa)	f_u/f_y	ϵ_{su}	f'_c (MPa)	f_t (MPa)
C1		150 × 1400 × 2800	G300E	300	409	1.36	18.1%	38.5	2.88
C1-1a C1-1b	Dimension	225 × 2100 × 4200	G300E	300	409	1.36	18.1%	38.5	2.88
C1-2a C1-2b		300 × 2800 × 5600	G300E	300	409	1.36	18.1%	38.5	2.88
C1-3	Reinforcement type	150 × 1400 × 2800	G500E	544	653	1.20	12.4%	38.5	2.88
C1-4		150 × 1400 × 2800	Class C	601	725	1.21	7.7%	38.5	2.88
C1-5	Strain hardening ratio	150 × 1400 × 2800	G300E	300	345	1.15	18.1%	38.5	2.88
C1-6		150 × 1400 × 2800	G300E	300	450	1.50	18.1%	38.5	2.88
C1-7	Concrete strength	150 × 1400 × 2800	G300E	300	409	1.36	18.1%	40.0	3.51
C1-8		150 × 1400 × 2800	G300E	300	409	1.36	18.1%	50.0	4.07
C1-9		150 × 1400 × 2800	G300E	300	409	1.36	18.1%	60.0	4.60

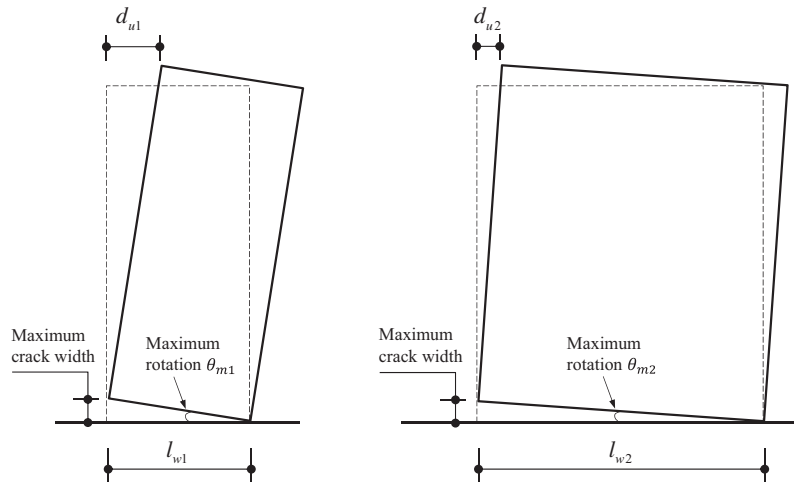


Fig. 13. Single crack model for lightly concrete walls.

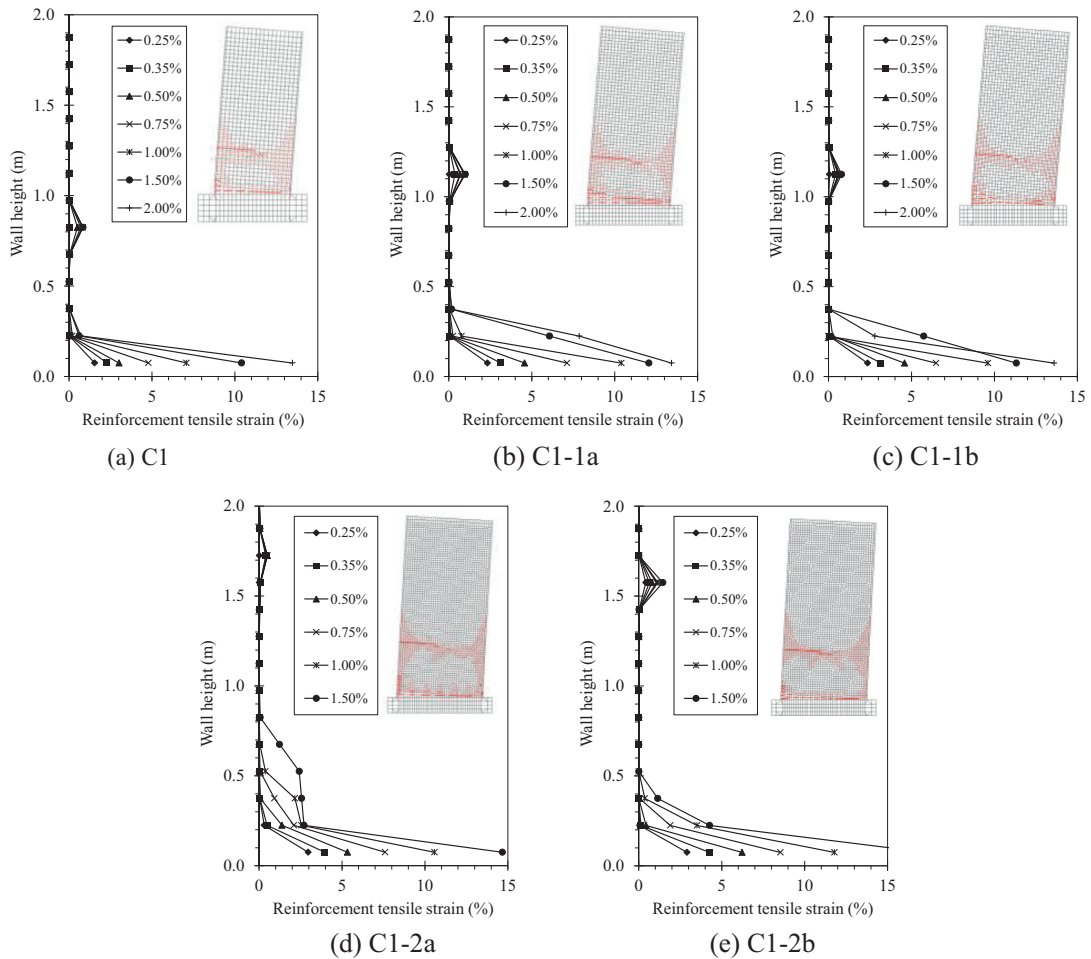


Fig. 14. Comparison of vertical reinforcement strain for walls with different sizes.

fracture earlier, as shown in Fig. 15. The lateral drifts when reinforcement was estimated to fracture were 1.83%, 1.65% and 1.22%, respectively. In addition, reinforcement spacing in the larger walls did not influence the crack pattern and drift capacity significantly. As shown in Fig. 15, the lateral drifts when reinforcement fractured were estimated to be 1.59% and 1.05% for walls C1-1b and C1-2b, respectively, which were similar with that of wall

C1-1a and C1-2a. The modelling results indicated that wall dimension was a key parameter to influence the seismic behaviour of lightly reinforced concrete walls with discrete cracking behaviour. The observation that the lateral drift capacity reduced as the wall dimensions increased in the modelled walls confirms the hypothesis proposed by Lu et al. [3] that a size effect is present for lightly reinforced concrete walls that are controlled by the

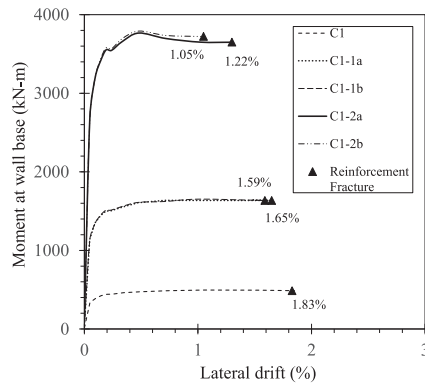


Fig. 15. Comparison of moment-drift curves for walls with different sizes.

formation of discrete flexural cracks. For the model results of walls C1, C1-1 and C1-2, the drift capacity did not decrease directly proportional to the wall dimensions because the modelled walls were not controlled by a single crack but instead exhibited 2–3 primary cracks. However, the drift capacity did decrease significantly as wall dimension increased and this finding implies that the tests reported by Lu et al. [3] may have overestimated the drift capacity of full scale lightly reinforced concrete walls. It is recommended that wall size and crack widths at which reinforcement occur be considered when assessing the seismic response of existing lightly reinforced concrete walls.

5.2. Reinforcement type

The behaviour of lightly reinforced concrete walls is also significantly dependent on the ductility and strain hardening ratio of the reinforcing steel because the crack distribution and reinforcement fracture are controlling parameters. In accordance with New Zealand standards, the earthquake grade G300E reinforcing bar used during the wall tests must have a uniform elongation at maximum strength greater than 15% and a strain hardening ratio (f_{ult}/f_y) greater than 1.15 [39]. Compared to higher strength G500E reinforcement also manufactured in New Zealand or other reinforcement types used around the world, G300E is regarded as high ductility reinforcing steel. In order to study the effect of reinforcement properties on the lightly reinforced concrete wall behaviour, walls with different reinforcement types, including G500E reinforcement, Class C reinforcement from Europe [40], and G300E with different strain hardening ratios were modelled and compared. The detailed reinforcement properties used for the modelled walls are summarised in Table 4. The vertical reinforcement ratio of the modelled walls was calculated in accordance with minimum vertical reinforcement requirements in NZS 3101 [1] which includes consideration for the yield strength of the reinforcement. Parameters including wall dimension, shear span ratio and axial load, concrete strength are all kept consistent with that of test wall C1.

Wall C1-3 (G500E) and C1-4 (Class C) were modelled and compared with wall C1 to investigate the effect of reinforcement type. To be consistent with test wall C1, the reinforcement properties for each grade were all derived from average test results rather than being lower characteristic or minimum values. The properties of G500E reinforcement were obtained from average test results by Pacific Steel in New Zealand and the properties of Class C were obtained from the reinforcing steel used for wall WSH3 tested by Dazio et al. [41]. As shown in Table 4, Class C and G500E reinforcement had lower ductility and strain hardening ratio when compared to the G300E reinforcement used during the wall tests. The

strain hardening ratio of Class C and G500E were both approximately 1.2, and the ultimate strain capacities were 7.7% and 12.4%, respectively.

A comparison of the calculated strains in the extreme tension vertical reinforcement of the modelled walls with different reinforcement types is shown in Fig. 16. The reinforcement strain profile prior to 1.0% lateral drift did not change significantly as the reinforcement type changed, indicating that the reinforcement type did not significantly affect the crack pattern. However, due to the difference of the reinforcement ductility, the ultimate drift capacities of these three walls were significantly different. Fig. 17-a shows the envelopes of the cyclic moment-displacement response of the three walls. The drift capacities when reinforcement was estimated to fracture for wall C1, C1-3 and C1-4 were 1.83%, 1.14% and 0.80%, respectively. Using G500E or Class C greatly decreased the drift capacity of the walls modelled, highlighting that the ultimate strain capacity (ductility) of the vertical reinforcement has a significant effect on the drift capacity of the lightly reinforced concrete walls.

Wall C1-5 and C1-6 were modelled to investigate the effect of the reinforcement strain hardening ratio. Three strain hardening ratios were investigated for G300E reinforcement, including 1.15 (C1-5), 1.35 (C1) and 1.5 (C1-6), representing lower limit, average, and upper limit allowable in accordance with AS/NZS 4671 [39]. From Fig. 16-a, d and e, it can be seen that the distribution in strains in the extreme tension vertical reinforcement varied significantly between walls C1, C1-5 and C1-6, indicating that the strain hardening ratio had a significant impact on the wall crack pattern. The larger the strain hardening ratio, the greater the number of secondary cracks, and the more evenly the reinforcement strains were distributed in the plastic hinge region. For example, as shown in Fig. 16-d and e, the reinforcement strains for wall C1-5 were predominantly concentrated on the wall base, whereas the reinforcement strains of wall C1-6 were more averagely distributed over the plastic hinge region. The larger strain hardening ratio provided a larger increase in strength in the reinforcement beyond yield which increased the likelihood of secondary cracks developing [2]. The increase in secondary cracking and more evenly distributed reinforcement strains also led to increased wall drift capacity as the strain hardening ratio increased. As shown in Fig. 17-b, the calculated ultimate drifts corresponding to reinforcement fracture were 1.59% and 1.83% for wall C1-5 and C1. For wall C1-6, the concrete in the compression region started to crush prior to reinforcement fracture due to the more evenly distributed vertical reinforcement strains that reduced the peak inelastic demand.

5.3. Concrete strength

Specified concrete strengths that represent lower characteristic values are typically used during structural design. However, it is recognised that the average strength of the supplied concrete and the strength increase beyond 28 days can often result in significantly higher concrete strengths in actual structures. For example, the specified 28-day concrete strength of the RC walls in the Gallery Apartment building that was damaged during the Canterbury Earthquake was $f'_c = 30$ MPa, but cores extracted from the building indicated that the actual compressive strength was closer to 50 MPa [38]. The average target compressive strength is often 20% greater than the specific strength and an additional 10% strength gain may occur over time [42]. Therefore, to investigate the effect of actual concrete strengths on the behaviour of lightly reinforced concrete walls, walls C1-7, C1-8, and C1-9 were modelled with concrete compressive strengths of 40 MPa, 50 MPa, and 60 MPa, respectively, representing specified, average long-term, and extreme concrete strengths. The *fib* model code recommendation was adopted to estimate the average uniaxial concrete

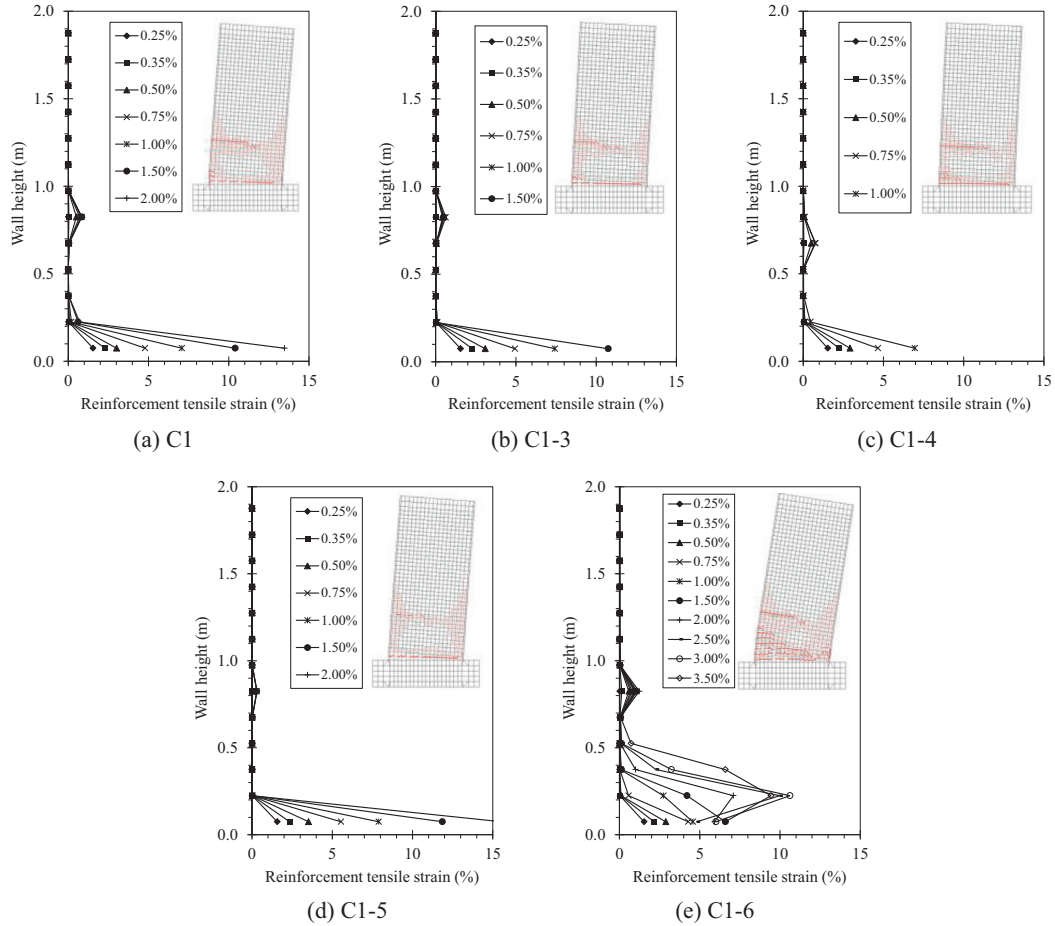


Fig. 16. Comparison of vertical reinforcement strain for walls with different reinforcement types.

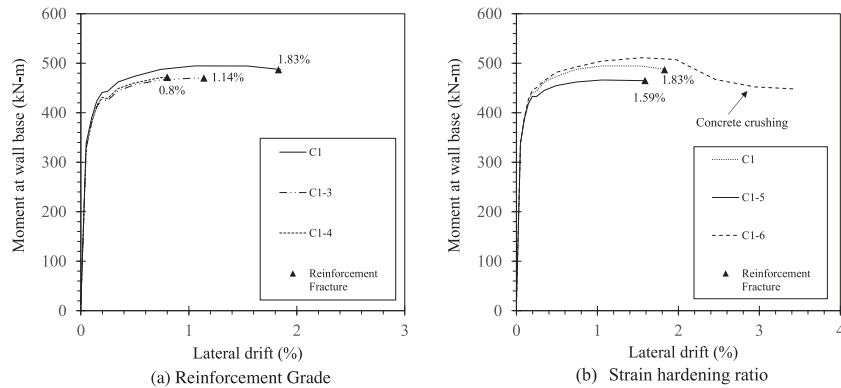


Fig. 17. Comparison of moment-drift curves for walls with different reinforcement types.

tensile strengths, which equated to 3.51 MPa, 4.07 MPa, and 4.60 MPa for walls C1-7, C1-8, and C1-9, respectively [31].

The calculated strains in the extreme tension vertical reinforcement and the envelopes of the cyclic moment-displacement response for the three walls modelled with different concrete strengths are compared in Figs. 18 and 19. The behaviour of wall C1-7 was similar with that of test wall C1, indicating that a slight increase in concrete strength from 38.5 to 40 MPa did not alter the behaviour significantly. However, for walls C1-8 and C1-9, the vertical reinforcement strains concentrated at a single flexural crack at the wall base. The reduction in flexural cracking was attributed to the higher concrete tensile strength that required a

larger reinforcement tension force to initiate secondary cracking. The reinforcement strain distributions were similar between C1-8 and C1-9 because the behaviour of both walls was dominated by the single flexural crack. The estimated ultimate drift capacities corresponding to reinforcement fracture were 1.81%, 1.68% and 1.60% for walls C1-7, C1-8, and C1-9, indicating that the drift capacity decreased as the concrete strength was increased. The results of these analyses confirmed that the variation of actual concrete strengths needs to be considered when assessing the seismic response of existing RC wall buildings as well as when developing minimum vertical reinforcement requirements to ensure that secondary cracks can occur within the plastic hinge region.

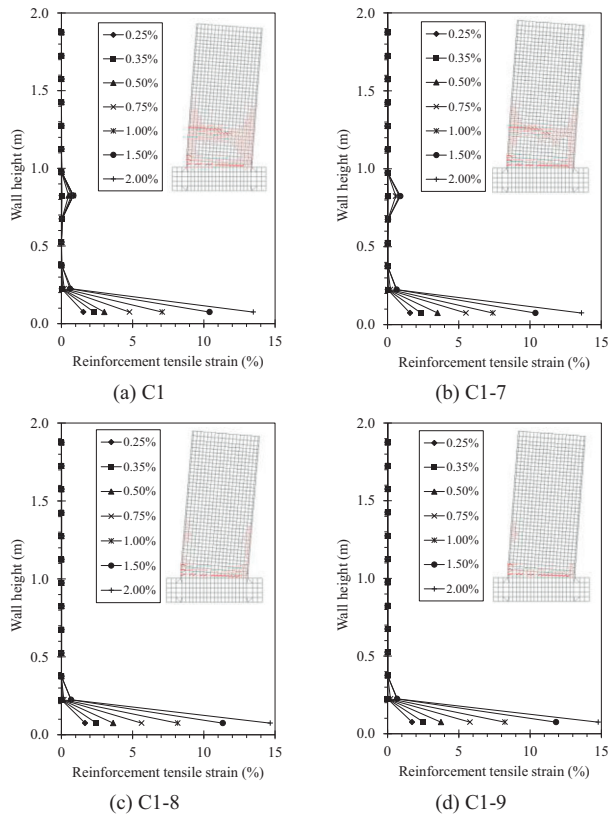


Fig. 18. Comparison of vertical reinforcement strain for walls with different concrete strength.

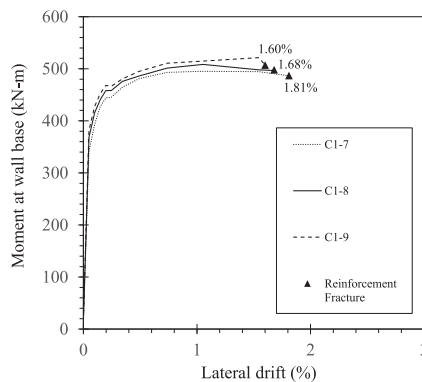


Fig. 19. Comparison of moment-drift curves for walls with different concrete strengths.

6. Conclusions

A detailed finite element model was developed to represent the behaviour of flexure dominant lightly reinforced concrete walls. The model developed was verified against experimental results from recent RC wall tests to establish the accuracy and limitations of the model. Finally, the effect of wall dimension, reinforcement properties, and concrete strength on the behaviour of lightly reinforced concrete walls was investigated using the model. The main conclusions drawn from this numerical study included:

- Refinement of the mesh size in the numerical model was essential to accurately capture the formation of discrete flexural cracks and localisation of reinforcement strains in the lightly reinforced concrete walls.

- The proposed model captured both the overall lateral load response and the local response parameters of the wall with good accuracy when considering the cyclic moment-displacement response, crack pattern, and vertical reinforcement strains.
- Buckling of the vertical enforcement was not accurately estimated in the model due to limitations of the reinforcement buckling model that did not account for the large tensile strain concentrations. However, the lateral drift at which reinforcement buckling initiated could be reliably estimated from the tensile strains calculated by the model.
- By using regularised reinforcement ultimate strains, the wall drift capacity when reinforcement fractured could also be reliably estimated from the tensile strains calculated by the model.
- Increased wall dimension had a significant effect on the drift capacity of the lightly walls modelled. When keeping reinforcement ratio and shear span ratio constant, the lateral drift capacity decreased as the wall length increased. As a result, the drift capacity in the lightly reinforced concrete walls tested by Lu et al. [3] may have been greatly overestimated due to their scale. It is recommended that wall size and crack widths at which reinforcement occur be considered when assessing the seismic response of existing lightly reinforced concrete walls.
- Using reinforcement with a higher yield strength and lower ductility did not significantly impact the crack pattern, but did greatly decrease the lateral drift capacity of the modelled walls. Furthermore, reducing the strain hardening ratio of the reinforcement resulted in a reduction in secondary cracking over the plastic hinge region and a significantly reduced lateral drift capacity. As a result, reinforcing steel strength and ductility must be accounted for when developing minimum vertical reinforcement provisions and when assessing the seismic response of existing lightly reinforced concrete walls.
- Concrete tensile strength had a significant influence on the cracking in the plastic hinge region of the modelled walls. Higher concrete strength resulted in fewer flexural cracks forming and reinforcement strain concentrating more significantly at the wall base, leading to reduced drift capacities. It is recommended that the average long-term concrete strength should be considered when assessing minimum vertical reinforcement requirements rather than relying on lower characteristic specified strengths.

Acknowledgements

The authors would like to acknowledge the funding provided by the Natural Hazards Research Platform (2012-UOA-03-NHRP), China Scholarship Council (CSC) and the Building Systems Performance Branch of the Ministry of Business, Innovation, and Employment (MBIE), in addition to project support and management provided by the UC Quake Center.

References

- NZS 3101:2006. Concrete structures standard (Amendment 2). Wellington, New Zealand: Standards New Zealand; 2006.
- Henry RS. Assessment of minimum vertical reinforcement limits for RC walls. Bull N Z Soc Earthquake Eng 2013;46(2):88–96.
- Lu Y, Henry RS, Gultom R, Ma QT. Cyclic testing of reinforced concrete walls with distributed minimum vertical reinforcement. J Struct Eng 2016 [in press], [http://ascelibrary.org/doi/abs/10.1061/\(ASCE\)ST.1943-541X.0001723?af=R](http://ascelibrary.org/doi/abs/10.1061/(ASCE)ST.1943-541X.0001723?af=R).
- Sritharan S, Beyer K, Henry RS, Chai YH, Kowalsky M, Bull D. Advancing seismic design of concrete walls through integration of field observations and research findings. Earthquake Spectra 2013;30(1):307–34.
- Wibowo A, Wilson JL, Lam NTK, Gad EF. Seismic performance of lightly reinforced structural walls for design purposes. Mag Concr Res 2013;65(13):809–28.

- [6] Belletti B, Damoni C, Gasperi A. Modeling approaches suitable for pushover analyses of RC structural wall buildings. *Eng Struct* 2013;57:327–38.
- [7] Orakcal K, Wallace JW. Flexural modeling of reinforced concrete walls – experimental verification. *ACI Struct J* 2006;103(2):196–206.
- [8] Panagiotou M, Restrepo JL, Schoettler M, Kim G. Nonlinear cyclic truss model for reinforced concrete walls. *ACI Struct J* 2012;109(2):205–14.
- [9] Jiang H, Kurama YC. Analytical modeling of medium-rise reinforced concrete shear walls. *ACI Struct J* 2010;107(4):400–10.
- [10] Kolozvari K, Orakcal K, Wallace J. Modeling of cyclic shear-flexure interaction in reinforced concrete structural walls. I: theory. *J Struct Eng* 2015;141(5):04014135.
- [11] Kwak HG, Kim DY. FE analysis of RC shear walls subject to cyclic loading. *Mag Concr Res* 2004;56(7):405–18.
- [12] Ghorbani-Renani I, Velev N, Tremblay R, Palermo D, Massicotte B, Léger P. Modeling and testing influence of scaling effects on inelastic response of shear walls. *ACI Struct J* 2009;106(3):358–67.
- [13] Luu H, Ghorbanirehani I, Léger P, Tremblay R. Numerical modeling of slender reinforced concrete shear wall shaking table tests under high-frequency ground motions. *J Earthquake Eng* 2013;17(4):517–42.
- [14] Dashti F, Dhakal R, PS. Numerical simulation of shear wall failure mechanisms. In: 2014 NZSEE Conference 2014; Auckland, New Zealand.
- [15] Wong SM, Vecchio FJ, Trommels H. *VecTor2 and formworks user's manual*. second ed. University of Toronto (Canada); 2002.
- [16] Vecchio FJ, Collins MP. Modified compression-field theory for reinforced concrete elements subjected to shear. *J Am Concr Inst* 1986;83(2):219–31.
- [17] Vecchio FJ. Disturbed stress field model for reinforced concrete: Formulation. *J Struct Eng* 2000;126(9):1070–7.
- [18] Palermo D, Vecchio FJ. Compression field modeling of reinforced concrete subjected to reversed loading: formulation. *ACI Struct J* 2003;100(5):616–25.
- [19] Almeida JP, Tarquini D, Beyer K. Modelling approaches for inelastic behaviour of RC walls: multi-level assessment and dependability of results. *Arch Comput Methods Eng* 2016;23(1):69–100.
- [20] Vecchio FJ, Lai D. Crack shear-slip in reinforced concrete elements. *J Adv Concr Technol* 2004;2(3):289–300.
- [21] Goodnight JC, Kowalsky MJ, Nau JM. Effect of load history on performance limit states of circular bridge columns. *J Bridge Eng* 2013;18(12):1383–96.
- [22] Seckin M. Hysteretic behaviour of cast-in-place exterior beam column subassemblies. Ann Arbor: University of Toronto (Canada); 1981. p. 1.
- [23] Dhakal RP, Maekawa K. Modeling for postyield buckling of reinforcement. *J Struct Eng* 2002;128(9):1139–47.
- [24] He XG, Kwan AKH. Modeling dowel action of reinforcement bars for finite element analysis of concrete structures. *Comput Struct* 2001;79(6):595–604.
- [25] Coleman J, Spacone E. Localization issues in force-based frame elements. *J Struct Eng* 2001;127(11):1257–65.
- [26] Pugh JS, Lowes LN, Lehman DE. Seismic design of concrete walled buildings. In: Second European conference on earthquake engineering and seismology, 2014; Istanbul.
- [27] Park R, Priestley MJN, Gill WD. Ductility of square-confined concrete columns. *ASCE J Struct Div* 1982;108(ST4):929–50.
- [28] Kupfer H, Hilsdorf HK, Rusch H. Behavior of concrete under biaxial stress. *ACI J* 1969;87(2):656–66.
- [29] Richart FE, Brandtzaeg A, Brown RL. A study of the failure of concrete under combined compressive stresses. Urbana, Illinois: Bulletin University of Illinois Engineering Experimental Station; 1928. p. 104.
- [30] Lee S-C, Cho J-Y, Vecchio FJ. Model for post-yield tension stiffening and rebar rupture in concrete members. *Eng Struct* 2011;33(5):1723–33.
- [31] Fédération Internationale du Béton (fib), fib Model Code for Concrete Structures. Fib model code for concrete structures 2010. Lausanne, Switzerland: Wiley-VCH Verlag GmbH & Co. KGaA; 2013.
- [32] Moyer MJ, Kowalsky MJ. Influence of tension strain on buckling of reinforcement in concrete columns. *ACI Struct J* 2003;100(1):75–85.
- [33] Restrepo-Posada JL. Seismic behaviour of connections between precast concrete elements PhD thesis. Christchurch (New Zealand): Department of Civil Engineering, University of Canterbury; 1992.
- [34] Waugh J, Aaleti S, Sritharan S, Zhao J. Nonlinear analysis of rectangular and T-shaped concrete walls. N.s. Foundation, editor; 2008. Report: ISU-ERI-Ames Report ERI-09327; Department: Department of Civil, Construction, Environmental Engineering; University: Iowa State University.
- [35] Chang GA, Mander JB. Seismic energy based fatigue damage analysis of bridge columns: Part 1 – evaluation of seismic capacity. N.T.R.N. NCEER-94-0006, Editor. Buffalo, N. Y: State University of New York; 1994.
- [36] Bosco C, Carpinteri A, Debernardi PG. Minimum reinforcement in high-strength concrete. *J Struct Eng (New York, NY)* 1990;116(2):427–37.
- [37] Rizk E, Marzouk H. New formula to calculate minimum flexure reinforcement for thick high-strength concrete plates. *ACI Struct J* 2009;106(5):656–66.
- [38] Holmes solutions, material testing in buildings of interest: gallery apartments, westpac centre and IRD building, 2011, Report prepared for the Canterbury Earthquakes Royal Commission: <<http://canterbury.royalcommission.govt.nz/documents-by-key/20111129.1351>>.
- [39] AS/NZS 4671:2001. Steel reinforcing materials. Sydney, Wellington: Standards Australia/Standards New Zealand; 2001.
- [40] CEN, Eurocode 2: Design of concrete structures—Part 1–1: General rules and rules for buildings, 1992-1-1:2004. Brussels: European Committee for Standardization.
- [41] Dazio A, Beyer K, Bachmann H. Quasi-static cyclic tests and plastic hinge analysis of RC structural walls. *Eng Struct* 2009;31(7):1556–71.
- [42] Cook D, Fenwick R, Russell A. Amendment 3 to NZS3101. In: The New Zealand Concrete Industry Conference 2014. Taupo; 2014.